BASIC SCIENCE

Nanomedicine: Nanotechnology, Biology, and Medicine
14 (2018) 1337–1347

Original Article

nanomedjournal.com

Promoting neuroregeneration by applying dynamic magnetic fields to a novel nanomedicine: Superparamagnetic iron oxide (SPIO)-gold nanoparticles bounded with nerve growth factor (NGF)

Muzhaozi Yuan, MS[a], Ya Wang, PhD[a,*], Yi-Xian Qin, PhD[a,b]

[a]*Department of Mechanical Engineering, State University of New York at Stony Brook, Stony Brook, NY, United States*
[b]*Department of Biomedical Engineering, State University of New York at Stony Brook, Stony Brook, NY, United States*

Received 3 November 2017; accepted 25 March 2018

Abstract

Neuroregeneration imposes a significant challenge in neuroscience for treating neurodegenerative diseases. The objective of this study is to evaluate the hypothesis that the nerve growth factor (NGF) functionalized superparamagnetic iron oxide (SPIO)-gold (Au) nanomedicine can stimulate the neuron growth and differentiation under external magnetic fields (MFs), and dynamic MFs outperform their static counterparts. The SPIO-Au core-shell nanoparticles (NPs) (Diameter: 20.8 nm) possessed advantages such as uniform quasi-spherical shapes, narrow size distribution, excellent stabilities, and low toxicity (viability >96% for 5 days). NGF functionalization has enhanced the cellular uptake. The promotion of neuronal growth and orientation using NGF functionalized SPIO-Au NPs, driven by both the static and dynamic MFs, was revealed experimentally on PC-12 cells and theoretically on a cytoskeletal force model. More importantly, dynamic MFs via rotation performed better than the static ones, i.e., the cellular differentiation ratio increased 58%; the neurite length elongation increased 63%.

Key words: Neuroregeneration; Nerve growth factor; SPIO-Au core-shell nanoparticles; Dynamic magnetic fields; Cytoskeletal force model

Due to the slow rate of axonal regeneration,[1] neuroregeneration, one of the most significant challenges in neuroscience, has driven extensive studies focused on techniques to increase the speed of neuron recovery. Many efforts have been contributed to develop the molecules,[2,3] proteins,[4,5] growth factors[6,7] and biomaterials[8,9] possessing the ability to stimulate or direct the axonal outgrowth. Among them, nerve growth factor (NGF) has been found to be essential for the neuronal growth and differentiation via the tropomyosin kinase receptor and the non-selective p75 neurotrophin receptor.[10,11] However, the slow diffusion and short half-life of NGF from the enzyme degradation[12,13] have restricted its application in neuroregeneration. Moreover, the main obstruction impeding its in-vivo studies is that many drugs designed for the treatment of nerve recovery like NGF cannot be easily transported through the blood brain barrier (BBB) due to the selective permeability of the BBB.[14] Therefore, it is necessary to find a suitable carrier to efficiently deliver nerve regenerative agents such as NGF across BBB and to enhance the half-life and efficiency of NGF in promoting neuronal growth.

Magnetic nanoparticles (NPs) have been extensively used in clinical practice, such as magnetic resonance imaging (MRI),[15–17] cell-labeling[18,19] and targeted drug or gene delivery[20] due to their special magnetic properties. Recent studies have examined the

Abbreviations: MF, magnetic field; D, diameter; nanoparticles, NPs; SPIO, superparamagnetic iron oxide; Au, gold; NGF, neuron growth factor; NGF-SPIO-Au, NGF functionalized SPIO-Au; BBB, blood brain barrier; MRI, magnetic resonance imaging; BNDF, brain derived neurotropic factor; DI, deionized; TEM, transmission electron microscopy; HS, horse serum; FBS, fetal bovine serum; DPBS, Dulbecco's phosphate-buffered saline; PLA, polylactic acid; FEM, finite element modelling; PLL, poly-L-lysine; ATCC, American Type Culture Collection.

Funding: This work was supported by the U.S. Department of Energy ARPA-E (DOE-AR0000531); the U.S. Office of Naval Research (ONR-N000141410230); the National Institutes of Health (R01 AR 52379 and AR 61821), and National Space Biomedical Research Institute through NASA Contract NCC 9-58.

The authors declare no conflict of interest.

*Corresponding author.
E-mail address: ya.s.wang@stonybrook.edu. (Y. Wang).

https://doi.org/10.1016/j.nano.2018.03.004
1549-9634/

Please cite this article as: Yuan M, et al, Promoting neuroregeneration by applying dynamic magnetic fields to a novel nanomedicine: Superparamagnetic iron oxide (SPIO)-gold nanoparticles bounded with nerve growth factor (NGF). *Nanomedicine: NBM* 2018;14:1337-1347, https://doi.org/10.1016/j.nano.2018.03.004

effect of iron oxide NPs as the nano carrier of NGF, and have shown the improvement of neurite outgrowth on PC-12 cell line.[21] M. Marcus et al[22] found the promotion effect of differentiation and neurite outgrowth of PC-12 cells and the extension of the NGF's half-life by conjugating NGF with iron oxide NPs. They have also proved the ability of iron oxide NPs to direct the neurite orientation.[23] Christina Riggio et al[24] confirmed that the NGF functionalized magnetic NPs can guide the neurite outgrowth along the external magnetic field (MF) direction by generating a tensile force under the applied MFs. It was also demonstrated that the effective delivery of brain derived neurotropic factor (BNDF) across the BBB can be achieved by using magnetic NPs as the nano-carriers, which enables the in-vivo application of BNDF.[14] however, none of the previous work involves the study of magnetic NPs driven by dynamic MFs.

Although magnetic NPs have been demonstrated as effective nano-carriers for NGF, for neuroregeneration, the direct use of uncoated magnetic NPs faces challenges such as their instability in neuron environment,[24–27] aggregations,[16] and the cellular toxicity.[28–31] To address these issues, magnetic NPs can be protected by a thin and impenetrable shell. Among various coating materials (polymer, alloy, metal, etc.),[32–34] gold (Au) was considered as the best candidate due to its outstanding biocompatibility,[35–39] high stabilities,[37,40] and tunable surface function.[41] Not only protects the iron oxide from exposure to complicated neuron environment, Au can also provide tunable surface functionalization with various of ligands such as proteins, aptamers and peptides through its stable thiol (-SH) and amide ($-NH_2$) binding affinity.[42–44] In our previous work, we have already shown the excellent biocompatibility of Au coated superparamagnetic iron oxide (SPIO) NPs in MC-3T3-E1 cell line by maintaining the cell viability as high as 97% for 7 days.[45]

In this work, to realize the precise control of neuroregeneration towards specific sites, a novel nanomedicine composed of NGF functionalized Au coated SPIO core NPs (Diameter (D): 20.8 nm) was synthesized and characterized. A non-invasive nerve regeneration technique was then developed by applying dynamic MFs on PC-12 cells treated with NGF functionalized SPIO-Au (NGF-SPIO-Au) NPs. The parametric effect on cell viability and cellular uptake was studied for cells treated with different concentrations and combinations of NGF and NGF-SPIO-Au NPs. Experimental results confirmed the dynamic MFs performed better than the static ones in neuroregeneration. Finally, the cytoskeleton force model was used to predict the neurite elongation and the orientation, which showed a good agreement with experimental data.

Methods

Synthesis of SPIO NPs

SPIO (Fe_2O_3) NPs were synthesized by the co-precipitation method.[40,46] Briefly, 2.81 g $FeCl_3^*6H_2O$ and 1.0 g $FeCl_2^*4H_2O$ were dissolved in a solution containing 1.03 g of 37% HCl in 12.5 ml of deionized (DI) water. The solution was added dropwise to 125 ml of 1.5 M NaOH solution with vigorous stirring. Then the formed black precipitate was isolated by magnetic decantation and washed 3 times with DI water, followed by dispersing the resulting Fe_3O_4 NPs in 125 ml of 0.01 M HNO_3 solution and heating the solution with stirring at 90°C for 30 min to oxidize the NPs. The resulting SPIO NPs were washed twice with DI water and dispersed in 125 ml of 0.1 M TMAOH.

Synthesis of SPIO-Au NPs

The 0.5 ml of as-synthesized SPIO NPs (60 mM) was sonicated and diluted to 1.5 mM with 19.5 ml of DI water. Then 5.5 ml of the diluted SPIO NPs was mixed with 5.5 ml of 0.1 M sodium citrate and stirred for 10 min to exchange the absorbed OH^- with citrate anions. Then the solution was diluted to 100 ml using DI water and followed by the addition of 0.5 ml of 1% $HAuCl_4$ solution to the mixture. The pH of the solution was adjusted to 8.86 by using 0.1 M NaOH solution. Then 0.6 ml of 0.2 M NH_2OH^*HCl was added to the mixture to form the Au coating. The color of the mixture was changed from brown to purple to pink-red in several minutes, which indicated the successful formation of the Au shell. Finally, the NPs was separated and washed by magnetic decantation. The as-prepared SPIO-Au NPs dispersed in 10 ml of DI water were directly used in the following experiments without any further purification. The concentration of the SPIO-Au NPs was 422 μg/ml (including 68.7% of Au in mass) (Table S1, supplementary material). All the aforementioned chemicals were purchased from Sigma-Aldrich (St. Louis, MO) unless otherwise states.

Functionalization of SPIO-Au NPs

NGF-β (N2513, Sigma) was labeled with Alexa Fluor 488 (A10235, Invitrogen) according to the manufacturer's protocol. The labeled protein was purified through a size exclusion purification resin to separate the unincorporated dye. The functionalization of the SPIO-Au NPs was performed by adding 14 μg of the labeled protein to 0.47 ml of 422 μg/ml SPIO-Au NPs (NGF: NPs = 1:14 in mass). The suspension was stirred for 3 h at room temperature. The resulting mixture was washed 3 times and the free NGF was removed using magnetic separation. Finally, the functionalized NPs was re-dispersed in 1 ml of DI water. To estimate the amount of NGF bounded to SPIO-Au NPs, the absorbance of the supernatant from the previous step was first measured at the absorbance peak of 280 nm (NGF). And then the concentration of free NGF was calculated by using a calibration curve showing the absorbance of a series of solutions with known NGF concentration. By subtracting the amount of free NGF, the final composition of 198 μg/ml of SPIO-Au NPs (68.7% Au in mass) and 11.15 μg/ml of NGF was achieved.

Characterization of SPIO-Au NPs

To observe the morphology of the synthesized SPIO-Au NPs, the transmission electron microscopy (TEM) imaging was performed on a JEOL JEM 1400 microscope at an operating voltage of 120 kV. Briefly, 100 μL droplets of each sample were dropped onto a 300-mesh copper grid (Ted Pella Inc., Redding, CA) and then left to dry in the air. The functionalization of SPIO-Au NPs was characterized by zeta-potential measurement using

Zetasizer Nano ZS (Malvern Instruments Inc., Westborough, MA). The measurements were repeated 3 times and the results were expressed using average values and standard deviations.

PC-12 cell culture

PC-12 cells (from rat pheochromocytoma) obtained from American Type Culture Collection (ATCC) were cultured in ATCC modified RPMI1640 medium supplemented with 10% heat inactivated horse serum (HS), 5% fetal bovine serum (FBS) and 1% penicillin–streptomycin (medium and supplements were purchased from Gibco, Grand Island, NY). Cells were cultured in poly-L-lysine (PLL, P4707, Sigma-Aldrich, St. Louis, MO) coated Petri dishes in a humidified incubator under a 5% CO_2 atmosphere at 37°C. To induce cell differentiation, PC-12 cells were incubated in serum reduced media (1% heat inactivated HS and 0.5% FBS).

Cell viability evaluations: Trypan blue exclusion assay and CCK-8 assay

To examine the cytotoxicity of SPIO-Au NPs, PC-12 cells were seeded into 24-well plates coated with PLL and incubated for 1 day. Then the cells were washed with Dulbecco's phosphate-buffered saline (DPBS) and incubated with SPIO-Au NPs at different concentrations (Groups: 0.7 μg/ml NGF, 10 μg/ml NPs, 0.2 μg/ml NGF-SPIO-Au NPs, 1 μg/ml NGF-SPIO-Au NPs, 5 μg/ml NGF-SPIO-Au NPs and 10 μg/ml NGF-SPIO-Au NPs). After 1, 3 and 5 days, the cells were dislodged from the dish, centrifuged and dispersed in growth medium. Cells were then stained with 0.4% Trypan blue solution (Gibco, Grand Island, NY) and examined through a hemocytometer (Bright-Line™ and Hy-Lite™ Counting Chambers, Hausser Scientific, PA). Cell cultured without NPs or NGF were used as control.

The CCK-8 cell counting kit (Sigma-Aldrich, St. Louis, MO) was used to evaluate the effect of SPIO-Au NPs on cell proliferation. PC-12 cells were seeded into PLL coated 96-well tissue culture plates at a density of $2*10^3$ cells/well with growth medium. After 24 h of incubation, the medium was replaced by fresh medium containing SPIO-Au NPs and (or) NGF (groups: 0.7 μg/ml NGF, 10 μg/ml NPs, 0.2 μg/ml NGF-SPIO-Au NPs, 1 μg/ml NGF-SPIO-Au NPs, 5 μg/ml NGF-SPIO-Au NPs and 10 μg/ml NGF-SPIO-Au NPs). Cells without NPs were seeded as a control group. After 1 and 3 days of incubation, the media were replaced with fresh media and 10 μL of CCK-8 solution was added to each well and followed by the incubation of the plates for 2 h at 37 °C. The absorbance was measured using a microplate reader (SpectraMax i3x, Molecular Devices Inc.) at the wavelength of 450 nm.

Cellular uptake TEM analysis

To study the cellular uptake of SPIO-Au NPs, PC-12 cells were seeded onto an Aclar® (Electron Microscopy Sciences Inc.) film in a 12-well plate at a density of $2*10^5$ cells per well and incubated with growth medium containing SPIO-Au NPs and NGF-SPIO-Au NPs at the concentration of 10 μg/ml. After 24 h of incubation, cells were prefixed in 3% Electron Microscopy grade glutaraldehyde in 0.1 M PBS, pH 7.4 at room temperature for 1 h. Cells were then fixed in 1% osmium tetroxide in 0.1 M PBS, pH 7.4, followed by the dehydration in a graded series of ethyl alcohol and embedded in Durcupan resin (Sigma-Aldrich, St. Louis, MO). Ultrathin sections (80 nm) were cut with a Leica EM UC7 Ultramicrotome (Leica Microsystems Inc.) and collected on formvar coated copper slot grids. Then these sections were stained with uranyl acetate and lead citrate and then analyzed by using a FEI Tecnai12 BioTwinG^2 microscope with an AMT XR-60 CCD digital camera system, at an accelerating voltage of 80 kV.

Neurite growth under dynamic MFs

To compare the cytoskeletal influence of dynamic MFs with static MFs, two identical magnetic applicators were printed on a MakerBot Replicator using a polylactic acid (PLA) filament. One applicator was used to generate static MFs. The other was installed on a rotating platform to generate dynamic MFs (Figure 1, *A* and *B*), where a Petri dish was mounted on a Tower Pro MG90S Micro Servo controlled by an Arduino Uno R3 Microcontroller A000066. The dish was rotated at 24 revolutions (45°) per minute during the test. Cells were seeded at the density of $2*10^5$ cells/dish in PLL pre-coated Ibidi Petri dishes (D: 35 mm). After 24 h, the medium was replaced by fresh serum reduced medium containing NGF-SPIO-Au NPs at the concentration of 10 μg/ml. Cells were incubated for 24 h to let the NPs to interact with cells. Then the Petri dish was put inside each magnetic applicator. Three groups of cells were prepared (control, static and dynamic). After 1 day, a light microscope (Axiovert 200M Inverted Fluorescence/phase Contrast Microscope (Carl Zeiss Inc.) equipped with an AxioCam CCD camera) was used to capture the images of differentiated cells. For each group, at least 40 pictures were acquired and more than 4000 cells were quantified. The neurite angle, length and number in each image were measured using Simple Neurite Tracer as a plugin of Fiji.

Statistical analysis

All results were analyzed based on at least 3 independent experiments and expressed using the standard deviation. Statistical analysis was performed by the Mann–Whitney *U* test and the one-way analysis of variance with Tukey post hoc test. Each group treated with SPIO-Au NPs was compared with the control group. *P* value less than 0.05 was considered as a significant difference.

Results

Characteristics

The TEM images showed the synthesized SPIO cores (Figure 2, *A*) (D: 13.2 ± 2.5 nm) before the coating process, and SPIO-Au NPs (Figure 2, *B*) (D: 20.8 ± 2.7 nm) with a quasi-spherical shape and a narrow size distribution. The light absorbance spectrum showed the peak of Au around 524 nm, confirming the existence of Au coating (Figure 3, *A*). The as-synthesized SPIO-Au NPs were then conjugated with Fluor 488 labeled NGF through S-N linkage. The UV-Vis measurement showed the typical absorbance peak of NGF protein and Fluor

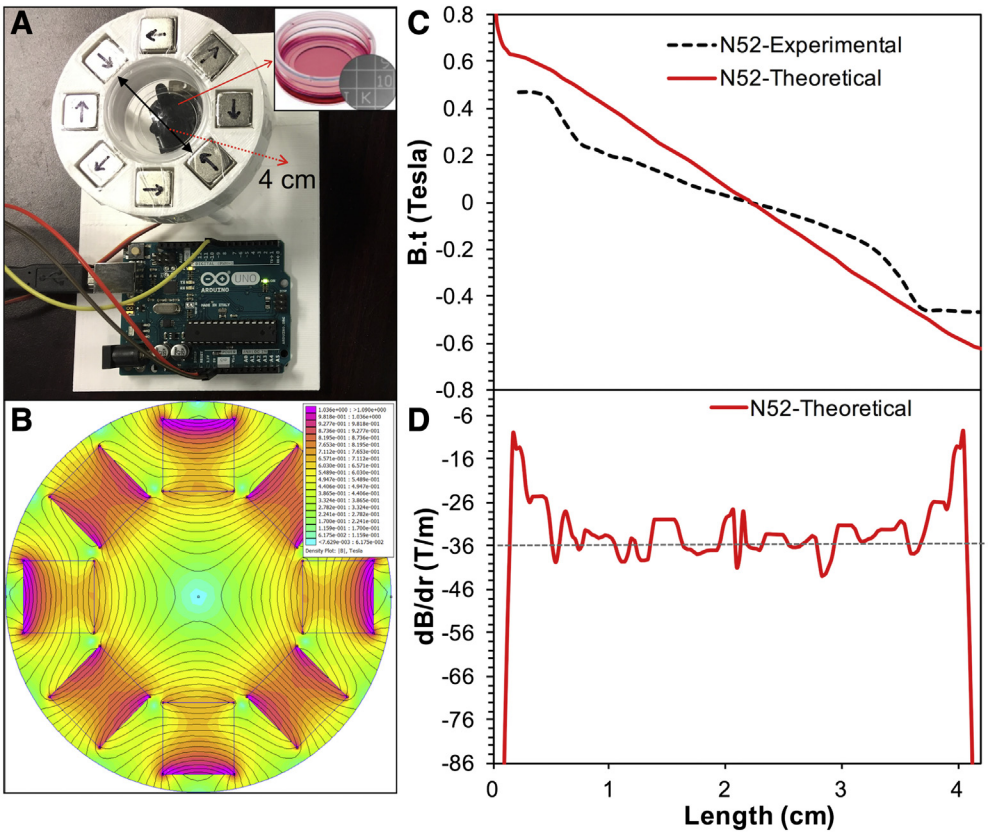

Figure 1. Set-up of the dynamic MFs. **(A)** The magnetic applicator using N52 magnets and the rotating platform. Inset: The Ibidi Petri dish **(B)** FEM of the N52 magnetic applicator; **(C)** FEM result (theoretical) and the experimental measurement of the flux density distribution inside the N52 Halbach-like magnetic applicator. **(D)** The derivative dB/dr (T/m) along the radial direction. The dot line in **(D)** represents the average value of dB/dr, which is −36.19 T/m.

488 at 280 nm and 494 nm respectively (Figure 3, *B*). The functionalization of SPIO-Au NPs with NGF was characterized by zeta potential measurement (Figure 3, *C*). The initial zeta potential of SPIO-Au NPs before the functionalization of NGF was −33.2 mV, reflecting the high stability of colloidal SPIO-Au NPs by strong electrostatic repulsion,[47] while it dropped to −25.1 mV with the addition of NGF (SPIO-Au: NGF = 1:0.005 in mass), which confirmed the successful functionalization of NGF with NPs. The zeta potential of NGF-SPIO-Au NPs increased towards the isoelectric point with higher NGF/SPIO-Au mass ratio, revealing that more of the NGF factors were bounded to SPIO-Au NPs and the saturation point was not reached in the tested range. Adversely, the hydrodynamic diameter decreased, implying the replacement of the original citrate ligand with NGF.

Cell viability evaluation

To reveal how SPIO-Au NPs affect the *in-vitro* cellular viability, the Trypan blue exclusion assay was performed on PC-12 cells treated with NGF (0.7 μg/ml), NPs (10 μg/ml) and NGF-NPs at the concentrations from 0.1 to 10 μg/ml. For up to 5 days of incubation, no significant reduction of live cells to total cells ratio was observed for all the concentrations compared with the control group. Interestingly, there was a significant increase of the viability for groups treated with NGF, NPs and NGF-NPs at 5 days of incubation (Figure 4, *A*). To further explain this phenomenon, the cell proliferation test using the CCK-8 colorimetric assay was performed. The absorbance of the formazan dye generated by the dehydrogenases activities in cells was recorded for each group, which was proportional to the number of live cells.[45] A stimulated proliferation (% of control group) was observed for groups treated with NGF, NPs and NGF-NPs. In particular, groups treated with NGF (184% of control, 7 days), NPs (166% of control, 7 days) and NGF-NPs (>163% of control, 7 days) had higher proliferation rate than the control group. And the proliferation rate was significantly improved with the increasing concentration of NGF-SPIO-Au NPs for up to 7 days of incubation. This increase explained why their viability from trypan blue assay also increased compared with the control group as more viable cells were proliferated relative to dead cells. (Figure 4, *B*)

Cellular uptake of NPs: TEM analysis

The cellular uptake of NPs and NGF-NPs at the concentration of 10 μg/ml was examined by TEM analysis on PC-12 cells incubated for 24 h (Figure 5). TEM images showed the successful internalization of NPs, locating inside the endosomal vesicles in the cytoplasm, rather than in the nucleus. The cytoplasmic membranes remained intact for both of the groups. For the cells treated with NGF-SPIO-Au NPs, the large clusters of NPs were found inside each cell with some of the NPs located

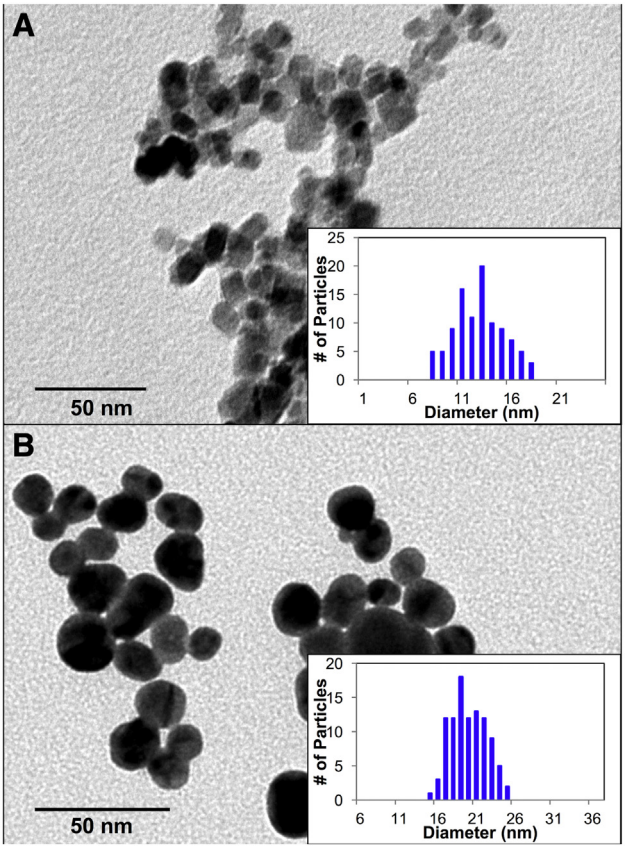

Figure 2. TEM images of the NPs. **(A)** SPIO NPs (13.2 nm); **(B)** SPIO-Au NPs (20.8 nm).

at the cell membrane which engulfing the NPs (Figure 5, *D*), implying the cellular uptake through endocytosis. While for the cells treated with SPIO-Au NPs only, smaller and less numbers of clusters of NPs were found as compared with the NGF functionalized NPs at the same concentration. Moreover, no SPIO-Au NPs were found at the cytoplasmic membrane, implying the different mechanism of cellular uptake.[48]

The morphology analysis: neuron growth and differentiation under static and dynamic MFs

To demonstrate our hypothesis that the NGF-SPIO-Au NPs can stimulate the neuronal growth and differentiation under external MFs, and the dynamic MFs outperform the static ones, PC-12 cells treated with NGF-SPIO-Au NPs (10 μg/ml) were cultured and placed in a dynamic magnetic applicator composed by eight of N52 NdFeB magnetic cubes of 0.5 inch arranged in a Halbach array (Figure 1, *A* and *B*) and a static magnetic applicator with the same magnetic configuration. In this setup, the magnetic strength along the diameter of the magnetic applicator was simulated from finite element modelling (FEM) and then experimentally measured using a F.W. Bell 8010 gauss/tesla meter (Figure 1, *C*), which was in agreement with the theoretical simulation. An average MF gradient of −36.19 T/m was calculated from the FEM result (Figure 1, *D*). In this test, we visualized the morphology of differentiated cells using bright field microscopy (Figure 6). Then the Fiji software was used to trace neurites for control (no MF: 1 Day-control-MF−), static (with static MFs: 1 Day-N52-static-MF+) and dynamic groups (with dynamic MFs: 1 Day-N52-dynamic-MF+). To quantify the orientation of neurite, the angle θ between the neurites and the direction of the magnetic force (radial outward direction) was measured and the orientation index was defined as Oi=cosθ ($0<\theta<\pi$, Oi~1 for neurite along the magnetic force direction).

As the results of analysis, after 1 day of magnetic treatment, both of the static (130%) and rotation (206%) groups showed a significant increase for the ratio of differentiated cells compared with the control group which had no magnetic treatment. Moreover, the dynamic group had much higher ratio (~158%) than that of the static group (Figure 7, *A*). The dynamic group also showed a significantly increased number of neurites per differentiated cells (117% of control) (Figure 7, *B*). Both of the static (114% of control) and dynamic (187% of control) groups exhibited longer average neurite length. Noticeably the average neurite length of the dynamic group was 63% longer than that of the static group (Figure 7, *C*). The distribution of angles between the neurite and the magnetic force (0°) showed that the neurites preferentially aligned along the direction of the magnetic force (Oi=0.20 for the static group and Oi=0.14 for the dynamic group), while in the control group without MFs, the neurites showed a homogeneous distribution with no preferred directions (Oi= 0.01) (Figure 8, *A*, *B*, *C*, and *D*). To analyze how the MF

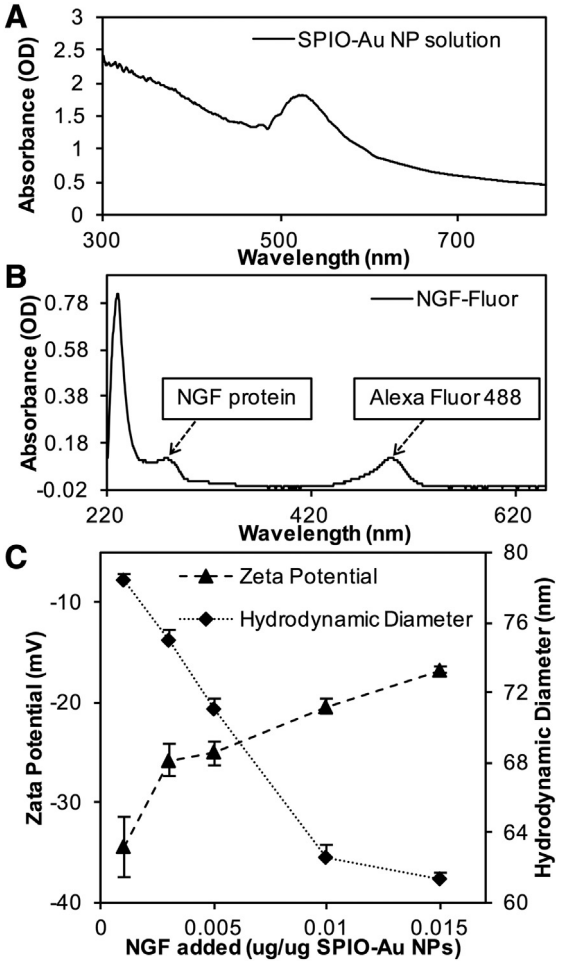

Figure 3. Light absorbance and zeta potential measurement. The UV-Vis spectrum of **(A)** SPIO-Au NPs and **(B)** NGF-Fluor. **(C)** Zeta potential of SPIO-Au NPs and hydrodynamic diameter at different NGF/NPs ratio.

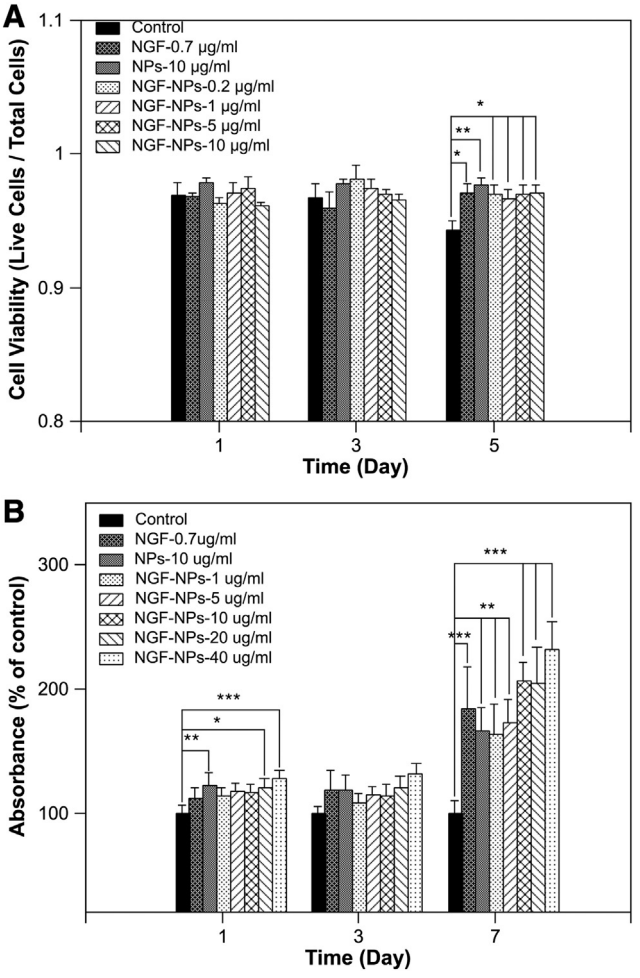

Figure 4. Cell viability evaluation. **(A)** The viability results from Trypan Blue staining. **(B)** The absorbance results from CCK-8 cell counting kit. The addition of NPs and NGFs significantly improved the cell proliferation for up to 7 days of incubation.

affected the neurite outgrowth, the neurite length (normalized with control) was compared for different MF configurations at different ranges of angle relative to the direction of the magnetic force. It was shown that under the dynamic MFs, the average neurite length was much higher than the group with static MFs at the angle between 0° and 50° (Figure 8, *E*).

The stimulation effect of the static magnetic force with NPs on the neuronal growth and differentiation was also validated in a Halbach-like magnetic applicator composed by eight of N42 NdFeB magnetic cubes of 0.5 inch (Figure S1, supplementary material, $dT/dr = -23.28$ T/m). It was shown that the ratio of differentiated cells significantly increased by 72%; the number of neurites per differentiated cells increased by 25%; the average neurite length increased by 43% of the control group, as well as the preferential alignment of the neurites along the direction of magnetic force (Figure S2 and S3, supplementary material). To reveal the relationship between the cell differentiation and the magnetic flux density, the distribution of the differentiated cells along the diameter of the magnetic applicator was plotted in Figure 8, *F*, which revealed the similar trend with the magnetic flux density.

Discussions

Our homemade SPIO-Au NPs were characterized with uniform shape, narrow size distribution, high stability, and facile functionalization with NGF. Although SPIO-Au NPs was proved to have no toxicity in other cell lines, such as mouse leukemic monocyte macrophage cells (36-56 nm, 1-500 μg/mL, > 90% viability, 3 days of incubation)[40] and MC-3T3-E1 cells (17 nm, 10-80 μg/mL, > 93% viability, 7 days of incubation), no viability or proliferation studies were reported on neuron-like cells, which can be essential for the application in neuronal regeneration. Here we confirmed their low cytotoxicity, and high biocompatibility in neuron-like cells, and their potentials in promoting neuron growth and differentiation.

The TEM analysis revealed two different cellular uptake mechanisms. For the cells treated with only SPIO-Au NPs at the concentration of 10 μg/mL, smaller clusters of NPs were found localized in the cytoplasm and no NPs were found at the endocytic pathway, implying that they may directly penetrate into the cells through diffusion. This mechanism has been

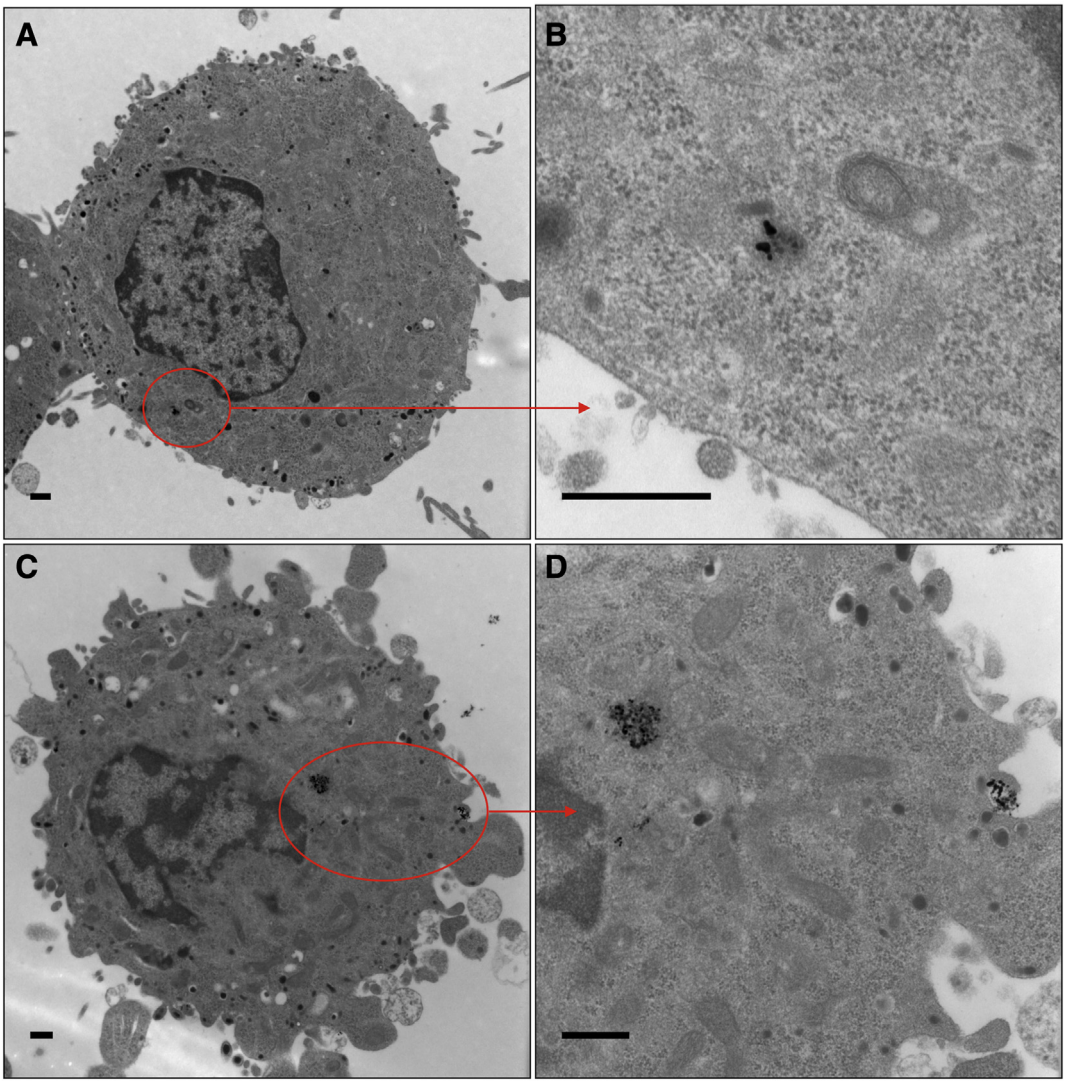

Figure 5. TEM images to show the cellular uptake of PC-12 cells. **(A)** and **(B)** PC-12 cells treated with NPs only; **(C)** and **(D)** PC-12 cells treated with NGF-NPs. **(B)** and **(D)** Enlarged images of areas shown inside the dashed circles in **(A)** and **(C)**. Scale bar = 500 nm

proposed by Mustafa et al[48] for Au NPs at the concentration as low as 10 μg/mL. However, when the SPIO-Au NPs were functionalized with NGF factors, they were more likely to cross the cytoplasmic membrane by endocytosis. To further identify which cellular uptake mechanism was (primarily) utilized, some commonly used inhibitors can be employed to study endocytic pathways, such as Chlorpromazine (to inhibit clathrin-mediated endocytosis), filipin III (to inhibit caveolae) and amiloride (to inhibit micropinocytosis). Detailed discussion will be presented in our future work.[49] By examining the existence of NPs inside the cells, the larger cluster and higher number of NGF functionalized NPs in PC-12 cells indicated that the addition of NGF promoted the cell absorption of NPs.

The morphology analysis in this study confirmed that driven by external magnetic forces, the NGF-SPIO-Au NPs can stimulate the neuronal differentiation, promote the axonal growth, and influence the neurite direction by aligning them toward the direction of the applied magnetic forces. Similar results have been obtained in literature for SPIO NPs driven by static MFs. However, none of the previous works reported the usage of dynamic MFs and examined their effect on neurons treated by NGF-SPIO-Au NPs. Our work innovatively introduced the dynamic MFs to NGF-SPIO-Au NPs for promoting neurite outgrowth. Experimental results proved that the dynamic MFs could remarkably enhance the neurite growth in comparison with the static ones.

To theoretically interpret the above results, it is necessary to establish a mechanical model to analyze NPs under forces. NPs' transport in biological systems is usually governed by several forces: magnetic force F_m, gravity F_g, viscous drag F_v, cytoskeletal force F_c, buoyancy force F_b and interparticle force F_{in}. For the NPs located inside the neurons, there is another type of force acting on NPs, called cytoskeletal force due to the elongation and the retraction of neurons. For most submicron particles with slow flow rate (<10 mm/s), the magnetic force and the cytoskeletal force dominant as all other forces can be neglected.[50]

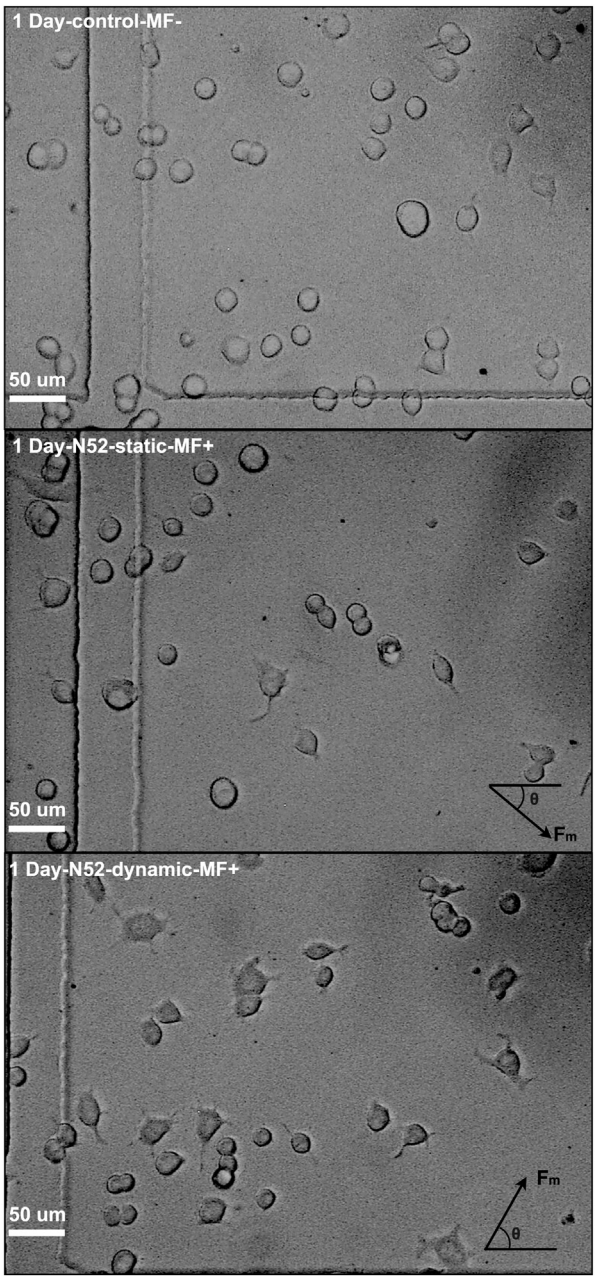

Figure 6. Bright field microscopy images. PC-12 cells were treated with 10 μg/ml NGF-SPIO-Au NPs **(A)** without MF, **(B)**with static and **(C)** with dynamic MF for 1 day of incubation.

For example, the gravity F_g can be expressed as

$$F_g = \rho_{particles}\frac{4}{3}\pi {r_{particles}}^3 g. \tag{1}$$

As our NPs are composed by SPIO core and Au coating, Eq. (1) can be rewritten as:

$$F_g = \rho_{SPIO}\frac{4}{3}\pi {r_{SPIO}}^3 g + \rho_{au}\frac{4}{3}\pi\left({r_{partices}}^3 - {r_{SPIO}}^3\right) g. \tag{2}$$

Here ρ_{SPIO} and ρ_{au} are 5240 kg m^{-3} and 19,320 kg m^{-3} as the density of SPIO and Au, respectively, r_{SPIO} (6.6 nm) is the radius of the SPIO core and $r_{partices}$ (10.4 nm) is the radius of the NPs. g is the gravitational acceleration near Earth's surface (9.81 m s^{-2}).

We can get $F_g = 2.73 * 10^{-19}$ N. With low Reynolds numbers, the viscous force can be expressed as

$$F_v = -6\pi\eta r_p\left(v_p - v_f\right). \tag{3}$$

Here η is the dynamic velocity of the fluid, v_p is the velocity of the particle, and v_f is the velocity of the fluid. In our experiment, the nanoparticles can be treated to be static, so this force can be neglected. The buoyancy force, F_b is given by:

$$F_b = \rho\frac{4}{3}\pi {r_{particles}}^3 g. \tag{4}$$

Here ρ is the density of the medium (approximated as the density of water 1000 kg m^3). The buoyancy force is calculated to be $2.1 * 10^{-20}$ N. Under an MF (**B**), the magnetic force F_m, on a particle is given by:

$$F_m = (m\cdot\nabla)\mathbf{B}. \tag{5}$$

Here m is the magnetic moment of the particle. Because the MF gradient d**B**/dr in our experiment is the only non-zero component, the Eq. (5) can be simplified to

$$F_m = m\frac{dB}{dr} = \frac{4}{3}\pi r_{particle}^3 \rho_{SPIO}\mathrm{M}\frac{d\mathrm{B}}{dr}. \tag{6}$$

Here, γ is the fraction of magnetic volume, M is the magnetization of particles (54.3 Am^2kg^{-1} from reference,[40] d**B**/dr is the MF gradient. We can get $F_m = 7.97*10^{-18}$ N for N42 magnets and $1.24*10^{-17}$ N for N52 magnet exerted on one NP.

To simulate the cytoskeleton force, the neurites can be modeled as Hookian springs with the spring constant k and an elongation of x. If there are n_{cells}^{NPs} NPs in the neuron, the cytoskeleton force per NP is:

$$F_c = \frac{kx}{n_{cells}^{NPs}}. \tag{7}$$

Here n_{cells}^{NPs} is roughly $2.5*10^5$ from literature.[24] From the experimental results the elongation of x for magnetic applicator with N42 magnets is 3.89 μm. When equilibrium is reached, the spring constant can be estimated as $5.12 * 10^{-13}$ N/μm. Using this simulation, we approximated the average elongation of neurites in the magnetic applicator with N52 magnets as 1.51 μm, which was very close to the experimental value of 1.394 μm. (Note: the cell density of the N52 case was 4 times of the N42 case. So n_{cells}^{NPs} was reduced to $0.625*10^5$ for the N52 case.)

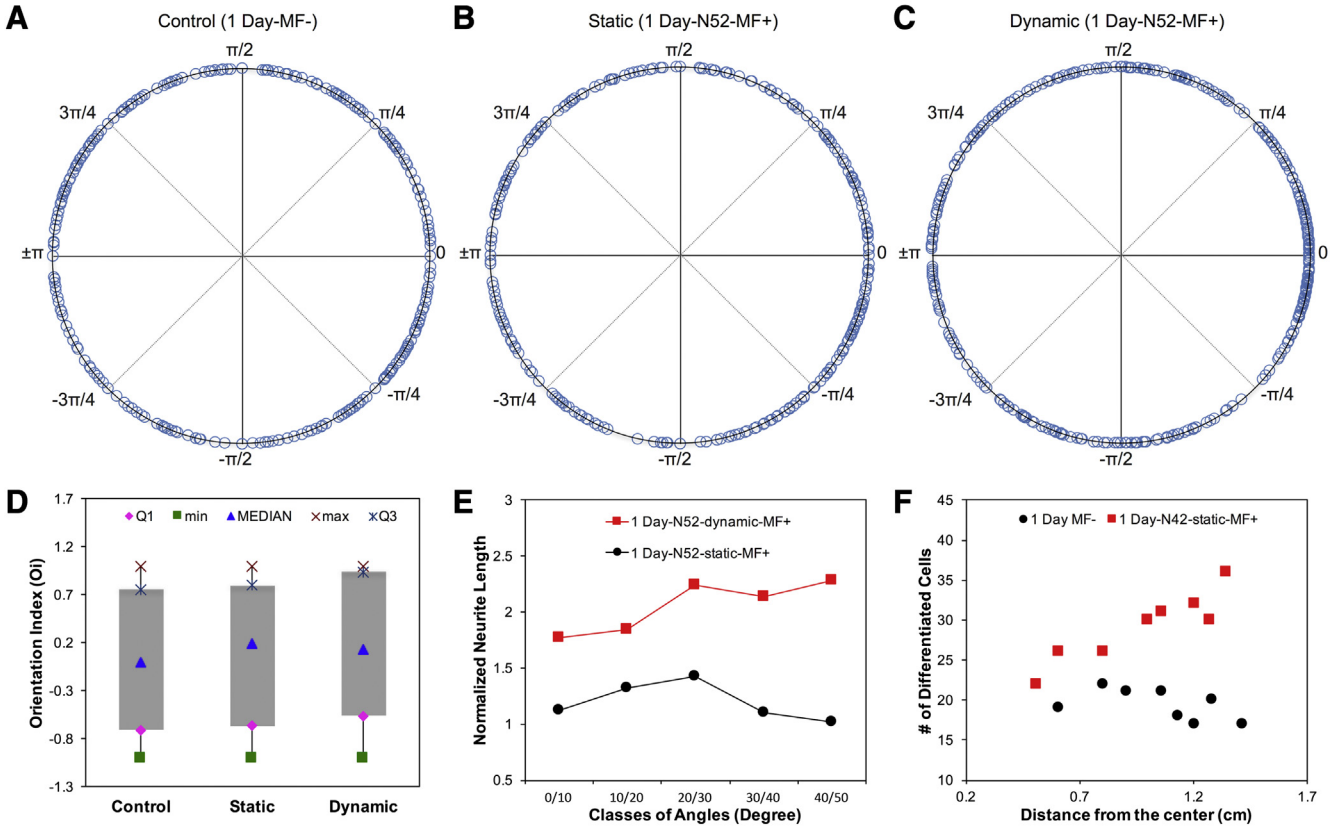

Figure 8. Neurite orientation (θ) distribution. **(A)** Without MF. **(B)** With static MFs. **(C)** With dynamic MFs. **(D)** Orientation index ($\cos\theta$) distribution: The box plot represents the median, the first quartile, the third quartile, the maximum and the minimum value. $\cos\theta$~1 for the neurites along the direction of magnetic force. **(E)** Average length of neurites normalized with the control grouped for different classes of angles of the neurites relative with the direction of the magnetic force (radial direction): The stimulated neurite growth aligned along the direction of the magnetic force with dynamic MFs. **(F)** The number of differentiated cells distributed throughout the dish (center at 0 cm): The number of differentiated cells increased with the higher magnetic flux.

The angle of the neurite can be simulated according to the equation:[24]

$$F^{\theta}_{neur}(\theta,t) = n^{NPs}_{neur} F_m sin = n^{NPs}_{cells} \frac{V_{neur}}{V_{cytop}} F_m sin = \frac{1}{3} k \Delta r \left[\left(\frac{l(t)}{a} \right)^2 - 1 \right]. \quad (8)$$

For $t = 0$, $\theta = \pi/2$ and for t_f =24 h, $\theta = \theta_f$. Taking experimental results of using N52 for example, the neurite length $l(t_f)$=1.394*10^{-6} m and k =4.1*10^{-6} N/m, which was calculated before. From the literature,[24] the neurite radius r = 7.5*10^{-7} m, the number of NPs per cell n^{NPs}_{cells} =2.5*10^5 and the parameter $a = \frac{1}{\sqrt{N_b}}$ =0.0045, where N_b=5*10^4 is the number of bridges for cell. Assume a uniform particle distribution in cell cytoplasm, the number of NPs entrapped in neurite n^{NPs}_{neur} can be estimated by knowing the volume of the neurite V_{neur}=2.46*10^{-18} m^3 and the volume of the cell cytoplasm V_{cytop}=4.41*10^{-16} m^3. By solving the Eq. (8), we found θ=82.8°, which was very close to the experimental measured value θ=78.5° (Oi=0.2). The modeling results allows the prediction the values of neurite elongation and the angle of the neurite orientation driven by a magnetic applicator formed by eight of N52 magnets, which are in good agreement with the experimental measurement. This model provides a predictive insight of the cellular effect induced by the cytoskeleton force.

This study confirms that applying dynamic MFs on NGF-SPIO-Au NPs is able to accelerate neurite growth by as high as 187% of control within only 24 h. This finding may be beneficial for the long-term nerve recovery and repair, and thus possesses the clinical importance to treat neurodegenerative diseases. Additionally, the ultra-small size of the SPIO-Au NPs (20.8 nm) is advantageous to transverse the BBB.[51] And the core-shell bimetallic structure makes them promising dual-mode contrast agents for multimode imaging technique, like MRI and computed tomography imaging.[40] It should be acknowledged that only one size of NPs is involved in this work, and future study will focus on the size dependence analysis. And we should also explore more variables like the strength of the MFs as well as the rotating speed and the angle of the dynamic MF, which may positively affect the development of neurites.

In this work, the SPIO-Au NPs (D: 20.8 ± 2.7 nm) were synthesized by combining co-precipitation and iterative hydroxylamine seeding method, and then functionalized with NGF. The light absorbance and zeta potential measurement confirmed the successful functionalization of NGF with NPs. The viability results (> 96%) indicated the excellent biocompatibility of SPIO-

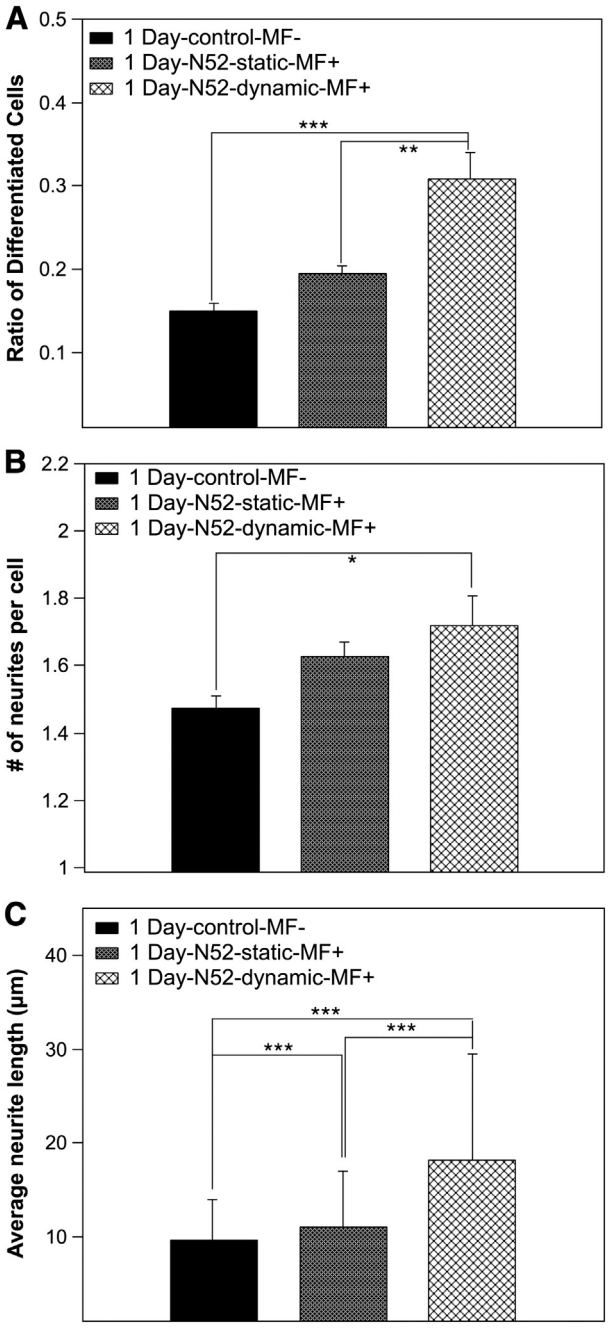

Figure 7. Morphology analysis for PC-12 cells treated with and without dynamic MFs. **(A)** Percentage of differentiated neuronal phenotype cells **(B)** Number of neurites per cell **(C)** Average neurite length; *$P < 0.05$; **$P < 0.01$; ***$P < 0.001$

Au NPs. The TEM images of PC-12 cells treated with NGF-SPIO-Au NPs showed that the cellular uptake can be enhanced by the functionalization of NGF. Then a noninvasive magnetic stimulation technique was developed by applying dynamic MFs on cells treated with NGF-SPIO-Au NPs. Our results showed that this multifunctional nanomedicine was able to effectively stimulate and promote the neuronal growth. And the dynamic MF was favored, as it drove the neurite stretching more efficiently than that of the static MF. Also a cytoskeleton force model was created, which agrees well with our experimental data of neurite elongation and orientation. This study confirmed the potential of non-invasive magnetic neuron stimulation technique synergistically combining the biocompatible magnetic NGF-SPIO-Au NPs with dynamic MFs for promoting neuronal growth.

Appendix A. Supplementary data

Supplementary data to this article can be found online at https://doi.org/10.1016/j.nano.2018.03.004.

References

1. Gordon T. The physiology of neural injury and regeneration: the role of neurotrophic factors. *J Commun Disord* 2010;**43**:265-73.
2. Dickson BJ. Molecular mechanisms of axon guidance. *Science* 2002;**298**:1959-64.
3. Alunni A, Bally-Cuif L. A comparative view of regenerative neurogenesis in vertebrates. *Development* 2016;**143**:741-53.
4. Lampe KJ, Antaris AL, Heilshorn SC. Design of three-dimensional engineered protein hydrogels for tailored control of neurite growth. *Acta Biomater* 2013;**9**:5590-9.
5. Yu N-K, Kim HF, Shim J, Kim S, Kim DW, Kwak C, et al. A transducible nuclear/nucleolar protein, mLLP, regulates neuronal morphogenesis and synaptic transmission. *Sci Rep* 2016;**6**:22892-902.
6. Babensee JE, McIntire LV, Mikos AG. Growth factor delivery for tissue engineering. *Pharm Res* 2000;**17**:497-504.
7. Faroni A, Mobasseri SA, Kingham PJ, Reid AJ. Peripheral nerve regeneration: experimental strategies and future perspectives. *Adv Drug Deliv Rev* 2015;**82**:160-7.
8. Orive G, Anitua E, Pedraz JL, Emerich DF. Biomaterials for promoting brain protection, repair and regeneration. *Nat Rev Neurosci* 2009;**10**:682-92.
9. Morelli S, Piscioneri A, Messina A, Salerno S, Al-Fageeh MB, Drioli E, et al. Neuronal growth and differentiation on biodegradable membranes. *J Tissue Eng Regen Med* 2015;**9**:106-17.
10. Aloe L, Rocco ML, Bianchi P, Manni L. Nerve growth factor: from the early discoveries to the potential clinical use. *J Transl Med* 2012;**10**:239 1-15.
11. Ziv-Polat O, Shahar A, Levy I, Skaat H, Neuman S, Fregnan F, et al. The role of neurotrophic factors conjugated to iron oxide nanoparticles in peripheral nerve regeneration: in vitro studies. *Biomed Res Int* 2014;**2014**:1-10.
12. Lee K, Silva EA, Mooney DJ. Growth factor delivery-based tissue engineering: general approaches and a review of recent developments. *J R Soc Interface* 2011;**8**:153-70.
13. Anitua E, Sánchez M, Orive G, Andia I. Delivering growth factors for therapeutics. *Trends Pharmacol Sci* 2008;**29**:37-41.
14. Pilakka-Kanthikeel S, Atluri VSR, Sagar V, Saxena SK, Nair M. Targeted brain derived neurotropic factors (BDNF) delivery across the blood-brain barrier for neuro-protection using magnetic nano carriers: an in-vitro study. *PLoS One* 2013;**8**e62241.
15. Yoffe S, Leshuk T, Everett P, Gu F. Superparamagnetic iron oxide nanoparticles (SPIONs): synthesis and surface modification techniques for use with MRI and other biomedical applications. *Curr Pharm Des* 2013;**19**:493-509.
16. Nam SY, Ricles LM, Suggs LJ, Emelianov SY. Imaging strategies for tissue engineering applications. *Tissue Eng Part B Rev* 2014;**21**:88-102.
17. Lalande C, Miraux S, Derkaoui SM, Mornet S, Bareille R, Fricain J-C, et al. Magnetic resonance imaging tracking of human adipose derived stromal

cells within three-dimensional scaffolds for bone tissue engineering. *Eur Cell Mater* 2011;**21**e54.
18. Ramaswamy S, Greco JB, Uluer MC, Zhang Z, Zhang Z, Fishbein KW, et al. Magnetic resonance imaging of chondrocytes labeled with superparamagnetic iron oxide nanoparticles in tissue-engineered cartilage. *Tissue Eng Part A* 2009;**15**:3899-910.
19. Saldanha KJ, Doan RP, Ainslie KM, Desai TA, Majumdar S. Micrometer-sized iron oxide particle labeling of mesenchymal stem cells for magnetic resonance imaging-based monitoring of cartilage tissue engineering. *Magn Reson Imaging* 2011;**29**:40-9.
20. Singh N, Jenkins GJS, Asadi R, Doak SH. Potential toxicity of superparamagnetic iron oxide nanoparticles (SPION). *Nano Rev* 2010;**1**:5358 1-15.
21. Kim JA, Lee N, Kim BH, Rhee WJ, Yoon S, Hyeon T, et al. Enhancement of neurite outgrowth in PC12 cells by iron oxide nanoparticles. *Biomaterials* 2011;**32**:2871-7.
22. Marcus M, Skaat H, Alon N, Margel S, Shefi O. NGF-conjugated iron oxide nanoparticles promote differentiation and outgrowth of PC12 cells. *Nanoscale* 2015;**7**:1058-66.
23. Marcus M, Karni M, Baranes K, Levy I, Alon N, Margel S, et al. Iron oxide nanoparticles for neuronal cell applications: uptake study and magnetic manipulations. *J Nanobiotechnol* 2016;**14**:37 1-12.
24. Riggio C, Calatayud MP, Giannaccini M, Sanz B, Torres TE, Fernández-Pacheco R, et al. The orientation of the neuronal growth process can be directed via magnetic nanoparticles under an applied magnetic field. *Nanomedicine* 2014;**10**:1549-58.
25. Cheng Y, Morshed RA, Auffinger B, Tobias AL, Lesniak MS. Multifunctional nanoparticles for brain tumor imaging and therapy. *Adv Drug Deliv Rev* 2014;**66**:42-57.
26. Cherukuri P, Glazer ES, Curley SA. Targeted hyperthermia using metal nanoparticles. *Adv Drug Deliv Rev* 2010;**62**:339-45.
27. Kumar CSSR, Mohammad F. Magnetic nanomaterials for hyperthermia-based therapy and controlled drug delivery. *Adv Drug Deliv Rev* 2011;**63**:789-808.
28. Mahmoudi M, Hofmann H, Rothen-Rutishauser B, Petri-Fink A. Assessing the in vitro and in vivo toxicity of superparamagnetic iron oxide nanoparticles. *Chem Rev* 2011;**112**:2323-38.
29. Yan H, Teh C, Sreejith S, Zhu L, Kwok A, Fang W, et al. Functional mesoporous silica nanoparticles for photothermal-controlled drug delivery in vivo. *Angew Chem Int Ed* 2012;**51**:8373-7.
30. Pinkernelle J, Raffa V, Calatayud MP, Goya GF, Riggio C, Keilhoff G. Growth factor choice is critical for successful functionalization of nanoparticles. *Front Neurosci* 2015;**9**:1-14.
31. Phan AD, Hoang TX, Nghiem THL, Woods LM. Surface plasmon resonances of protein-conjugated gold nanoparticles on graphitic substrates. *Appl Phys Lett* 2013;**103**:163702-6.
32. Biju V. Chemical modifications and bioconjugate reactions of nanomaterials for sensing, imaging, drug delivery and therapy. *Chem Soc Rev* 2014;**43**:744-64.
33. Wang L, Park H-Y, Lim SII, Schadt MJ, Mott D, Luo J, et al. Core@shell nanomaterials: gold-coated magnetic oxide nanoparticles. *J Mater Chem* 2008;**18**:2629-35.
34. Alkilany AM, Thompson LB, Boulos SP, Sisco PN, Murphy CJ. Gold nanorods: their potential for photothermal therapeutics and drug delivery, tempered by the complexity of their biological interactions. *Adv Drug Deliv Rev* 2012;**64**:190-9.
35. Kawazoe N, Chen G. Gold nanoparticles with different charge and moiety induce differential cell response on mesenchymal stem cell osteogenesis. *Biomaterials* 2015;**54**:226-36.
36. Heo DN, Ko W-K, Bae MS, Lee JB, Lee D-W, Byun W, et al. Enhanced bone regeneration with a gold nanoparticle–hydrogel complex. *J Mater Chem B* 2014;**2**:1584-93.
37. Xu Z, Hou Y, Sun S. Magnetic core/shell Fe3O4/Au and Fe3O4/Au/Ag nanoparticles with tunable plasmonic properties. *J Am Chem Soc* 2007;**129**:8698-9.
38. Connor EE, Mwamuka J, Gole A, Murphy CJ, Wyatt MD. Gold nanoparticles are taken up by human cells but do not cause acute cytotoxicity. *Small* 2005;**1**:325-7.
39. Albanese A, Chan WCW. Effect of gold nanoparticle aggregation on cell uptake and toxicity. *ACS Nano* 2011;**5**:5478-89.
40. Zhang S, Qi Y, Yang H, Gong M, Zhang D, Zou L. Optimization of the composition of bimetallic core/shell Fe2O3/Au nanoparticles for MRI/CT dual-mode imaging. *J Nanopart Res* 2013;**15**:1-9.
41. Mahmoudi M, Sant S, Wang B, Laurent S, Sen T. Superparamagnetic iron oxide nanoparticles (SPIONs): development, surface modification and applications in chemotherapy. *Adv Drug Deliv Rev* 2011;**63**:24-46.
42. Zhou H, Zou F, Koh K, Lee J. Multifunctional magnetoplasmonic nanomaterials and their biomedical applications. *J Biomed Nanotechnol* 2014;**10**:2921-49.
43. Maleki H, Simchi A, Imani M, Costa B. Size-controlled synthesis of superparamagnetic iron oxide nanoparticles and their surface coating by gold for biomedical applications. *J Magn Magn Mater* 2012;**324**:3997-4005.
44. Conde J, Ambrosone A, Sanz V, Hernandez Y, Marchesano V, Tian F, et al. Design of multifunctional gold nanoparticles for in vitro and in vivo gene silencing. *ACS Nano* 2012;**6**:8316-24.
45. Yuan M, Wang Y, Qin YX. SPIO-Au core-shell nanoparticles for promoting osteogenic differentiation of MC3T3-E1 cells: concentration-dependence study. *J Biomed Mater Res A* 2017;**105**(12):3350-9.
46. Lyon JL, Fleming DA, Stone MB, Schiffer P, Williams ME. Synthesis of Fe oxide core/Au shell nanoparticles by iterative hydroxylamine seeding. *Nano Lett* 2004;**4**:719-23.
47. Vijayakumar S. In vitro stability studies on gold nanoparticles with different stabilizing agents. *Int J Curr Sci* 2014;**11**:84-93.
48. Mustafa T, Watanabe F, Monroe W, Mahmood M, Xu Y, Saeed LM, et al. Impact of gold nanoparticle concentration on their cellular uptake by MC3T3-E1 mouse osteoblastic cells as analyzed by transmission electron microscopy. *J Nanomed Nanotechnol* 2011;**2**:1000118 1-7.
49. Nam HY, Kwon SM, Chung H, Lee S-Y, Kwon S-H, Jeon H, et al. Cellular uptake mechanism and intracellular fate of hydrophobically modified glycol chitosan nanoparticles. *J Control Release* 2009;**135**:259-67.
50. Darbyshire PM. Dynamics of magnetic nanoparticles in newly formed microvascular networks surrounding solid tumours: a parallel programming approach. *Cancer Res* 2016;**4**:9-23.
51. Masserini M. Nanoparticles for brain drug delivery. *ISRN Biochem* 2013;**2013**:1-18.